Three - Dimensional Magnetotelluric Inversion Using Generalized RRI Method

Kazunobu YAMANE[1], Shinji TAKASUGI[2],
Hee Joon KIM[3] and Ki Ha LEE[4]
1)Geothermal Energy Research and Development Co., Ltd., Tokyo 103-0026, Japan.
2)JMC Geothermal Engineering Co., Ltd., Tokyo 103-0016, Japan.
3)Pukyung National University, Pusan 608-737, Korea.
4)Lawrence Berkeley National Laboratory, CA 94720, U.S.A

Abstract

To handle the real geological environment, 3-D MT inversion studies has been developed by many researchers(Madden et al, 1989; Mackie et al, 1993). The method to calculate 3-D Frechte derivative takes enormous computational time and computer memory, while the RRI method(Smith and Booker, 1991), the approximate one, provides reasonable solution with less computing resource. But it may be liable to the static shift.

The method discussed here is expanding the RRI method into the local 3-D area. We have developed a generalized method based on a locally three dimensional analysis to improve the computational efficiency and stablility of inversion. The developed algorithm has been realized in the GRRI3D code, which has been tested on synthetic 3-D MT data. The case study includes interpretation of 3-D MT survey conducted in the Minami-kayabe area located in the southern part of Hokkaido, Japan.

Introduction

Three-dimensional MT inversion continues to be a challenging problem in electromagnetic exploration. Recently, 3-D MT inversion has been reported to investigate 3-D geological environments. Most of these studies, however, require enormous computational efforts. One of promising approaches may be the rapid relaxation inversion (RRI) reported by Smith and Booker(1991). In this method the actual inversion is carried out for each column in 1-D fashion. The forward modeling used may be rigorous, so that as iteration is continued one hopes to have the lateral effects gradually accounted for.

Lee et al. (1995) and Yamane et al. (1998) presented an efficient approach to the 2-D inversion of MT data by generalizing the RRI method. The generalized RRI (GRRI) scheme does not require additional computation time when compared with the original RRI scheme, but it should converge faster and may be less likely getting caught in local minima. This is because the GRRI involves a locally 2-D analysis, whereas the inversion part of the original RRI is strictly 1-D. We have extended the GRRI scheme, using the approach suggested by Xie (1996, personal commu.), to solve 3-D MT problems.

In this paper it is expected that the data structure be completely in the form of tensor impedance and admittance, and the base of data encompasses over a 2-D surface area. In the initial development of 3-D MT inversion scheme, we use the finite-difference forward code developed by Mackie et al. (1994). However, the inversion code named GRRI3D should be able to utilize any 3-D forward code as long as it is efficient in terms of computing speed

with reasonably accurate modeling results.

Minami-kayabe MT data set is used for 3-D inversion analysis. Before this inversion, we reprocessed the time series of observed MT data with the cascade decimation in order to improve the quality of the tensor impedance.

Minami-Kayabe MT Survey

The New Energy and Industrial Technology Development Organization (NEDO) has been conducting a "Geothermal Development Promotion Survey" in the Minami-Kayabe area located in southern Hokkaido, Japan. Since the exploitation of near-surface geothermal resources is expected in this area, surface geological surveys have been carried out and seven wells approximately 1,000 m deep have been drilled. In 1988 MT and AMT soundings were conducted in the Minami-Kayabe area using the "High Accuracy MT System" developed by NEDO. The locations of the MT measurement sites are shown in Figure 1. In this survey 161 sites were arranged in a square lattice like shape. The electric dipoles were continuous in the lattice area.

Two remote sites, LD-1 and LD-2, were located northeast of the survey area for remote-reference processing. Since the topography of the survey area is very rugged, a complete lattice arrangement of MT sites was not possible.

In both the MT and AMT soundings, data were acquired for two components of the electric field (E_x and E_y) and three components of the magnetic field (H_x, H_y, H_z). The measurement frequencies for the MT soundings ranged from 0.01 Hz to 250 Hz. AMT data were acquired over a range of 130 Hz to 20,000 Hz, using the SD (synchronous detection) mode.

Generally, in MT measurements, the intensities of natural electromagnetic fields are very low, and the signals are easily contaminated by some form of a electrical noise. In order to obtain results of high quality, it is necessary to acquire and stack a large amount of data. Local noise is generally removed by conducting simultaneous measurements at different sites, and then use a remote-reference processing technique (Gamble et al., 1979).

In conventional FFT processing, the time series data are divided into segments consisting of a number of data points (the number being a power of 2, usually 512 or 1024). When the coherency for a segment is smaller than a preset threshold value, this segment is not used in the estimation of the power spectra. Consequently, the number of stacks is usually reduced. This often causes greater variances of the estimated values. To obtain accurate spectra over a wide frequency band, large-volume data processing is necessary. For this, the FFT method is time-consuming. Therefore, we employed the cascade decimation method, which is suitable for fast calculations over a wide frequency band like Minami-kayabe area.

After the time series data were processed using the cascade decimation method and the Fourier coefficients were obtained, power spectra were calculated. The data were sorted by the multiple coherency between appropriate horizontal field components in this time. The multiple coherency of a dual input and single output linear system is represented by the following equation.

$$O_i = G_{ix} I_x + G_{iy} I_y \ (i = x \text{ or } y)$$

This is given in terms of auto and cross spectra of the inputs and output (I_x, I_y, O_i) as

$$C^2_{I\cdot Oi}=\frac{|\langle IO_i^*\rangle|^2\langle I_xI_x^*\rangle+|\langle IO_i^*\rangle|^2\langle I_yI_y^*\rangle-2Re\{\langle IO_i^*\rangle\langle IO_i^*\rangle\langle I_xI_y^*\rangle\}}{\langle O_iO_i^*\rangle\{\langle I_xI_x^*\rangle\langle I_yI_y^*\rangle-|\langle I_xI_y^*\rangle|^2\}}$$

$$(i=x \text{ or } y)$$

The asterisk(*) indicates the complex conjugate. The multiple coherency is unity if I_x, I_y and O_i are noise free, and it decreases to zero with increasing noise in any components. For the present data processing we calculate four multiple coherencies.

$$C^2_{H\text{-}Ex},\ C^2_{H\text{-}Ey},\ C^2_{E\text{-}Hx},\ and\ C^2_{E\text{-}Hy}$$

In our processing scheme, a coherency-sorting algorithm was added to the original cascade decimation. First, incoming data are passed through operator-specified minimum amplitude screening criteria, based on the magnetic field amplitude of 6th and 8th Fourier coefficients from the cascade decimation. The auto power spectra and cross power spectra are calculated from the Fourier coefficients and sorted in temporary storage at each level of decimation. When the number specified for averaging is reached at a given level of decimation, four multiple coherencies are calculated for each harmonic. The average of the spectra is then sorted and accumulated into a file based on the value of the geometric mean of the H-E_x and E-H_y coherencies and of the H-E_y and E-H_x coherencies. The storage file into which the temporary spectral averages are sorted is divided into ten bins, each containing complete data sets from which MT parameters can be calculated, with different data quality based on the multiple coherencies.

In parallel with the cascade decimation processing remote reference processing was also conducted. The remote reference processing method, which was proposed by Gamble (1979), has proved to be quite effective in MT measurements and is now widely used.

In Japan, however, where the level of cultural noise is quite high, this method is often insufficient to reduce the noise to a satisfactory level. Therefore a triple reference processing method, in which two reference sites are used, was also applied (Takasugi et al, 1992).

Theoretical Description of Inversion

From Maxwell's equation in the frequency domain, one derives the following Helmholtz equation in terms of the electric field.

$$\nabla\times\nabla\times\mathbf{E}+i\omega\mu\sigma\mathbf{E}=0\,. \tag{1}$$

Taking the perturbation of this equation with respect to the conductivity, we obtain

$$\nabla\times\nabla\times\delta\mathbf{E}+i\omega\mu\sigma\delta\mathbf{E}=-i\omega\mu\delta\sigma\mathbf{E}\,. \tag{2}$$

Suppose that the 3-D model is divided into a set of vertical prisms (Figure 2). We choose nine neighboring prisms as the basic inversion unit. This unit consists of the volume V whose surface boundary is composed of top boundary (TBV) and four side boundaries (SBV). The bottom boundary may be ignored since we will assume that electric and magnetic field

are negligibly small.

Now we define an test function, E*, such that

$$\mathbf{E}^* = \begin{cases} \mathbf{E} & \text{in } V_1, \\ \mathbf{0} & \text{on } SBV, \end{cases} \tag{3}$$

Multiplying the perturbed field equation (2) by the test function E* and integrating over the volume, we get.

$$\int_V (\nabla \times \nabla \times \delta\mathbf{E} + i\omega\mu\sigma\delta\mathbf{E}) \cdot \mathbf{E}^* dv = -\int_V i\omega\mu\delta\sigma\mathbf{E} \cdot \mathbf{E}^* dv \tag{4}$$

Integrating by parts of the equation, or applying the Green theorem, this equation is broken into

$$\oint_{BV} [(\mathbf{n} \times \nabla \times \delta\mathbf{E}) \cdot \mathbf{E}^* - (\mathbf{n} \times \nabla \times \mathbf{E}^*) \cdot \delta\mathbf{E}] da + \int_V (\nabla \times \nabla \times \mathbf{E}^* + i\omega\mu\sigma\mathbf{E}^*) \cdot \delta\mathbf{E} dv$$
$$= -\int_V i\omega\mu\delta\sigma\mathbf{E} \cdot \mathbf{E}^* dv \tag{5}$$

where **n** is a unit vector outward normal to BV(Figure 2). According to the definition of test function **E*** described by equation (3), equation (5) is finally reduced to

$$\begin{aligned} \int_{V_1} \delta\sigma(E_x^2 + E_y^2 + E_z^2) dv = & \int_{TBV} \left[(\delta H_y E_x^* - \delta H_x E_y^*) + (\delta E_y H_x^{**} - \delta E_x H_y^{**}) \right] da \\ & + \frac{1}{i\omega\mu} \oint_{SBV} (\mathbf{n} \times \nabla \times \mathbf{E}^*) \cdot \delta\mathbf{E} da \\ & - \int_{V_2} \left(\sigma\mathbf{E}^* + \frac{\nabla \times \nabla \times \mathbf{E}^*}{i\omega\mu} \right) \cdot \delta\mathbf{E} dv \\ & - \int_{V_2} \delta\sigma(E_x E_x^* + E_y E_y^* + E_z E_z^*) dv \end{aligned} \tag{6}$$

We limit the only unknown t o be the conductivity variation in the central prism V_1 on right-hand side of above equation. If the prism V_1 consists of K blocks, a discretized version of equation(6) is

$$\sum_{k=1}^{K} C_v(x_i, y_j, z_k; \omega)\, \delta m(x_i, y_j, z_k) = S, \tag{7}$$

Here, δ m is the incremental change in the log conductivity for each element in V_1.
C is the kernel of the integral equation.

Synthetic Test

In order to test the effectiveness of this inversion scheme, we selected a simple model. The synthetic model is shown in Figure 3. Two conductive prisms are surrounded by

homogeneous earth with 100 ohm-m. The frequencies used for this model are 1000, 500, 200, 100, 50, 20 and 10Hz. The inverse model used here comprises 324 (= 18 × 18) columns of 20 × 20 × 315 m, and each column has ten layers. The inversion procedure is repeated until a misfit between the measured and modeled data is reduced to an acceptable level of rms misfit (S), which is given by

$$S = \sqrt{\frac{1}{N}\sum_{i=1}^{N}\frac{\left\|\mathbf{Z}_i^m - \mathbf{Z}_i^d\right\|^2}{\left\|\mathbf{Z}_i^d\right\|^2}}, \tag{8}$$

where $\|\bullet\|$ denotes the determinant, $\mathbf{Z}$ is the impedance tensor, and the superscripts m and d indicate the modeled and measured data, respectively. If we choose an appropriate damping factor, then a reasonable inversion result can be obtained after several iterations. Figure 4 shows an example of successful inversion, and the inverted image was obtained after ten iterations. The residual error was reduced from 0.01 to 0.001 and changed insignificantly after ten iterations as shown in Figure 5. From Figure 3 we can find that the two conductors are clearly identified. In the inversion all the resistivity parameters are constrained to positive values.

3-D Structure of Minami-Kayabe Field

Minami-kayabe area is underlain mostly by Neogene and Quaternary formation. The outcrops of Pre-Tertialy basement rocks are not seen in this area. The Neogene zone comprise the Miocene Shidomarigawa formation (volcanic and sedimentary rocks) and the Pliocene Isoya pyroclastic rocks. The Quaternary zone is represented by Pleistocene volcanic rock. Neogene insrusive rocks prevail in the east of the area.

We use MT data for total 60 MT soundings in the inversion. The frequencies of MT data range from 0.5 Hz to 256 Hz. Data below 0.5 Hz is neglected. This is because the data quality is poor due to large contamination DC noise. The starting model is a homogeneous earth with 100 ohm-m.

The convergence of inversion (RMS misfit versus iteration number) is shown in Figure 6. Figure 7 shows the inverted image, and a whole view of the inverse model. The computation time was about 50 minutes on IBM PC (333 MHz).

A relatively conductive zone(20 ohm-m or less) is extensively found at the depth from 70m to 400m. This zone seems to correspond to the Shiodomarigawa formation, because it is widely distributed at these levels. On the other hand, a resistive zone may be dominant below this formation. However, this 3-D inversion profile does not indicate a resistive zone because lower frequencies are neglected in this time. These conductive zones may be attributed to the presence of a clay mineral due to hydrothermal alteration.

Conclusion

We applied the 3-D MT inversion algorithm for the simple synthetic model and Minami-kayabe geothermal field. At first stage, the intensive data processing using the cascade decimation was carried in order to have a high quality impedance data stood for 3-D analysis. A large contamination of DC noise, however, distorted lower frequency impedance. This situation prevented us from delineating the basement structure. But a shallow

resistivity structure is corresponded to the alternated zones, which play as a cap rock of geothermal reservoir.

The algorithm of the MT inversion described here is similar to the GRRI method employed for the 2-D MT inversion. The test function is forced to take zero value on the four side boundaries of nine prisms inversion unit to render the resulting perturbation equation easy to handle. This method will result in an approximation conductivity mapping. But, it is possible to reconstruct a 3-D resistivity images with a small amount of computer resources.

We could not delineate the deep subsurface structure of Minami-kayabe geothermal field, while shallow resistivity distribution must be regarded as an alternated zone.

Reference

Gamble,T.D., Goubau,W.M, and Clarke,J, Magnetotellurics with a remote magnetic reference, *Geophysics*, 44, 53-68,1979

Lee, K. H., G. Xie, K. Yamane, and S. Takasugi, A new 2-D inversion scheme for magnetotelluric data using a modified RRI method, *Proc. World Geothermal Congress,* Florrence, Italy, 1995.

Mackie, R. L., and T. R. Madden, Three-dimensional magnetotelluric inversion using conjugate gradients, *Geophys. J. Int.*, 115, 215-229, 1993.

Mackie, R. L., J. T. Smith, and T. R. Madden, Three-dimensional electromagnetic modeling using finite difference equations: The magnetotelluric example, *Radio Sci.*, 29, 923-925, 1994.

Madden,R. L., and Mackie, R. L, Three-dimensional magnetotelluric modeling and Inversion, *Proc. IEEE*, 77,318-331,923-925

Smith,J.T and Booker,J.R, Rapid inversion of two- and three-dimensional magnetotelluric data, *J.Geophys.Res.*, 96, 3905-3922

Takasugi, S., K. Tanaka, N. Kawakami, and S. Muramatsu, High spatial resolution of resistivity structure revealed by a dense network MT measurement—a case study in the Minamikayabe area, Hokkaido, Japan, *J. Geomag. Geoelectr.*, 44, 289-308, 1992.

Yamane, K., S. Takasugi, K. H. Lee, and Y. Ashida, A new magnetotelluric inversion scheme using generalized RRI method and case studies, *Butsuri-Tansa*, 51, 141-153, 1998.

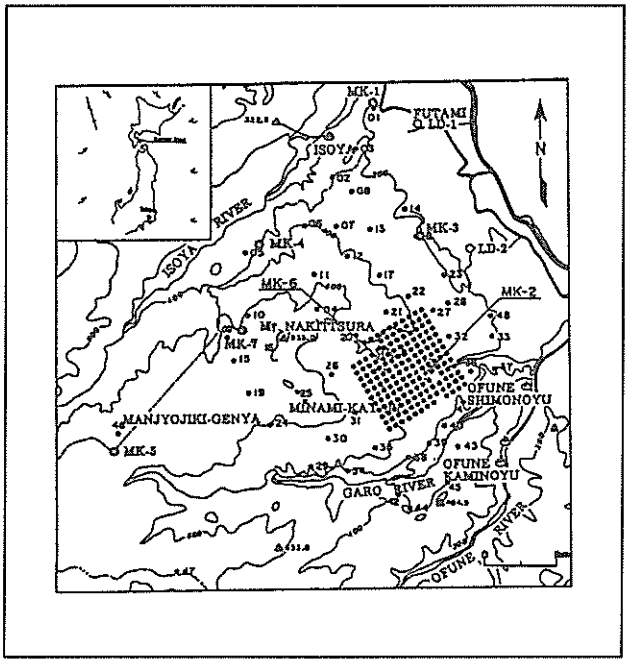

Figure 1. MT sites in Minami-kayabe area. The solid circles show the local MT sites and open circles indicate the remote reference sites at LD-1/2.

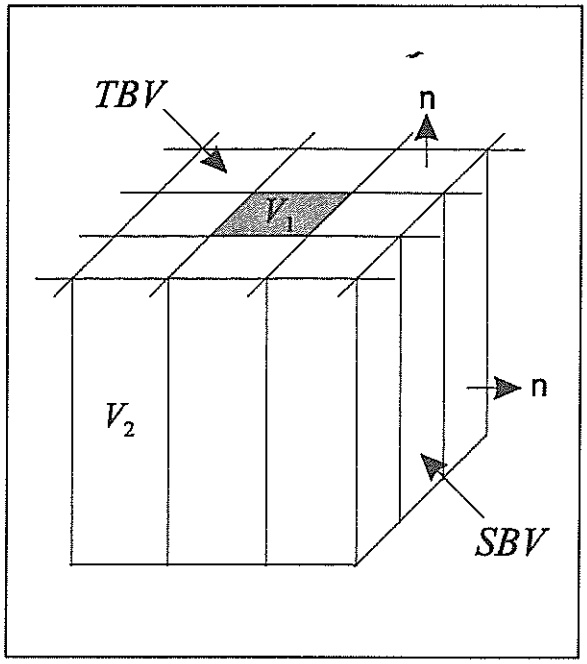

Figure 2. A nine-prism inversion unit. Eight side prisms surround the central prism. The total the central prism. The total volume of the inversion unit is V=V1+V2, where V 1 is the volume of the central prism and V2 the outer eight prisms surrounding. The boundary of the inversion unit consists of top (TBV) and side (SBV) boundaries.

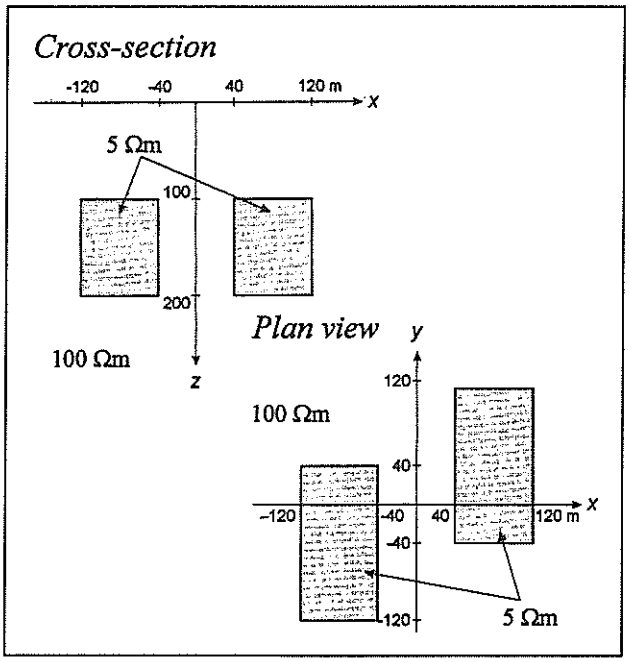

Figure 3. The 3-D model used to generate synthetic MT data. Two conductive bodies of 5 ohm·m are buried in uniform medium of 100 ohm·m.

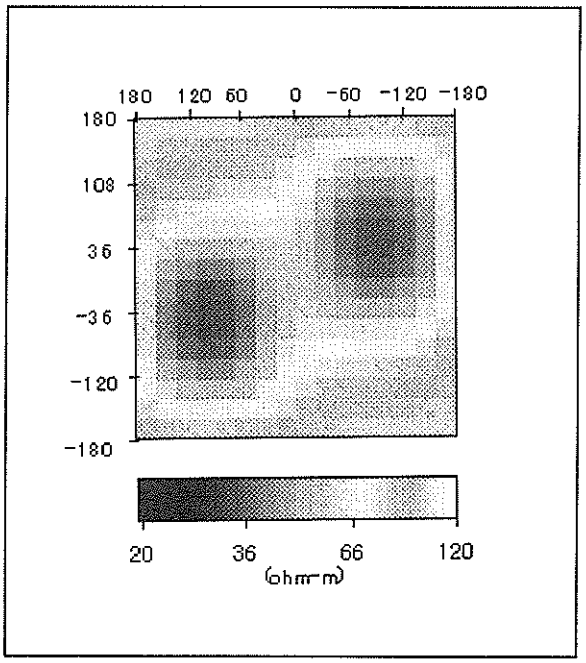

Figure 4. Inversion result of the synthetic MT data at the 180m depth.

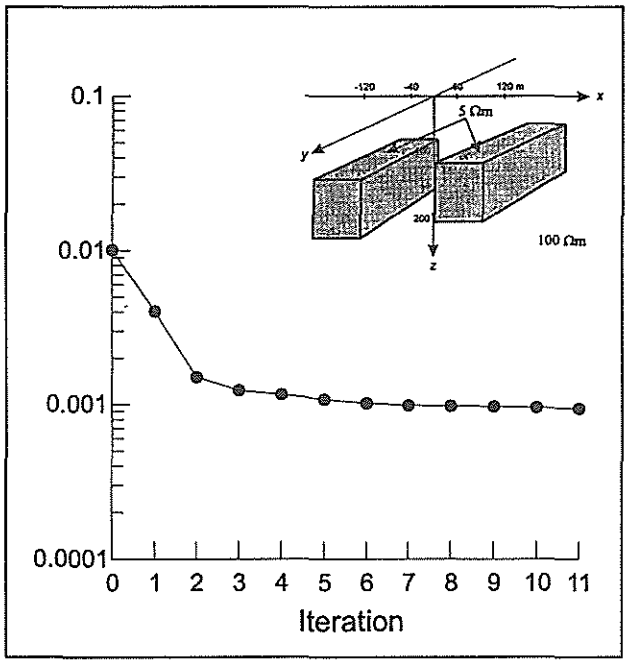

Figure 5. The RMS misfit progression of the synthetic model

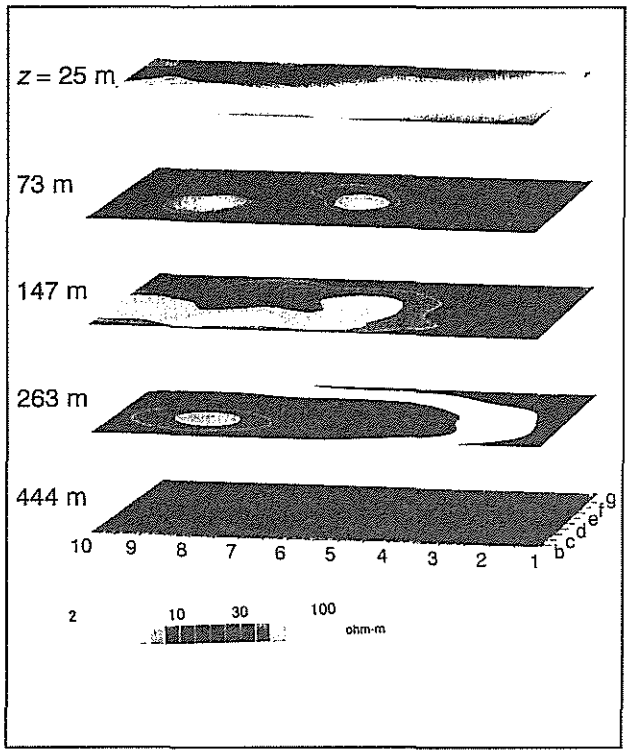

Figure 7. The inverse results of MT data in the Minami-Kayabe area.

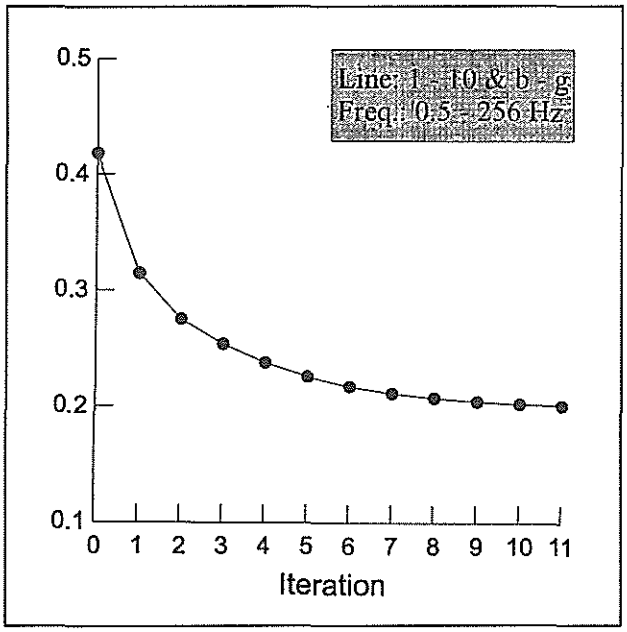

Figure 6. The convergence of the inversion.